ACS Photonics

pubs.acs.org/journal/apchd5

Article

Spin Coherence and Relaxation Dynamics of Localized Electrons and Holes in $FAPbI_3$ Films

Guillaume Lagüe, Frederick Bernardot, Victor Guilloux, Laurent Legrand, Thierry Barisien, Jesús Sánchez-Diaz, Sergio Galve-Lahoz, Imen Saïdi, Kais Boujdaria, Juan P. Martinez-Pastor, Christophe Testelin, Iván Mora-Seró, and Maria Chamarro*

Cite This: https://doi.org/10.1021/acsphotonics.4c00632

Read Online

ACCESS | Metrics & More | Article Recommendations | Supporting Information

ABSTRACT: We obtained highly stable polycrystalline thin films of $FAPbI_3$ prepared under air ambient conditions. In these materials, the presence of Pb−O bonds prevents the propagation of α- to δ-$FAPbI_3$ phase conversion and allowed addressing the study of the spin coherence and spin relaxation dynamics of the photogenerated carriers. We studied, at 2 K, the coherent evolution of electronic spins in $FAPbI_3$ films by measuring the photoinduced Faraday rotation (PFR) under a transverse magnetic field. We identified two contributions to the measured signal that we associated with localized electrons and holes. The study of the Larmor spin precession as a function of magnetic field leads to Landé factors $|g_e| = 3.447 \pm 0.006$ for electrons and $|g_h| = 1.134 \pm 0.003$ for holes. We measured long spin coherence times of localized electrons (holes) of 3.3 ns (2.4 ns). PFR measurements in a longitudinal magnetic field yielded a carrier spin relaxation time of 17 ns at 32 mT. Finally, we were interested in experimentally estimating the value of the Kane energy, which is the key parameter to determine the band structure and the optical properties of halide perovskites, as well as the interaction of these materials with a magnetic field. From the experimentally determined hole g-factors and low-temperature absorption spectrum, we obtain the Kane energy parameter of $FAPbI_3$, $E_P = 13.1$ eV, a value slightly smaller than the calculated one $\tilde{E}_P = 14.7$ eV. We, thus, experimentally establish a bridge between the optical and spin properties of halide perovskites.

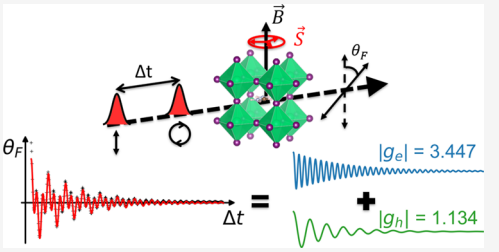

KEYWORDS: *lead halide perovskites, $FAPbI_3$ polycrystalline films, photoinduced Faraday rotation, spin dynamics*

INTRODUCTION

For more than a decade, solar cells based on halide perovskites (HP) have been setting new photovoltaic efficiency records.[1] As a result, a great interest in these materials, with the aim of discovering the key to their success, has grown. Indeed, they have brought to light outstanding optical properties:[2] strong absorption and bright luminescence, a tunable energy gap and exciton binding energy by adjusting the chemical composition. Their electronic properties are also very interesting: good bipolar transport, large carrier diffusion distances, low formation energies for shallow defect states, and small thermal conductivity at room temperature. For photovoltaic applications, $CH_3NH_3PbI_3$ ($MAPbI_3$) is the flagship material, which combines a cheap and easy fabrication by a low-temperature solution process and a theoretical yield of photovoltaic conversion efficiency of approximately 30%, which is close to the maximum expected for a single-junction solar cell. $MAPbI_3$ has also very quickly gained an important place in other applications and scientific fields such as optoelectronics and spintronics. For example, the long carrier lifetimes and low nonradiative recombination rates were taken advantage of when demonstrating optically pumped laser emission in $MAPbI_3$ nanowires.[3] The first studies on spin relaxation and decoherence in HP have been performed in $MAPbI_3$ films[4,5] and revisited later.[6−9] This opened the field to other studies on spin dynamics in HP materials[10,11] and has revealed interesting effects[12−15] and differences with more conventional semiconductors.[16]

In principle, $NH_2CH{=}NH_2Pb_2I_3$ ($FAPbI_3$) would be a better candidate than $MAPbI_3$ for single-junction solar cells because its band gap has the lowest energy among the Pb-based HP family. The very promising α-phase (also known as the black phase) of $FAPbI_3$ is, however, difficult to stabilize at room temperature. Recently, different groups have implemented a strategy to make it stable, and some of them have obtained promising results.[17,18] The difficulties to stabilize the material have so far prevented exploring the whole peculiarities and characteristics of $FAPbI_3$ in photovoltaic and beyond photovoltaic applications. $FAPbI_3$, as other members of the HP family, is a highly promising material not only in the

Received: April 4, 2024
Revised: June 27, 2024
Accepted: June 28, 2024

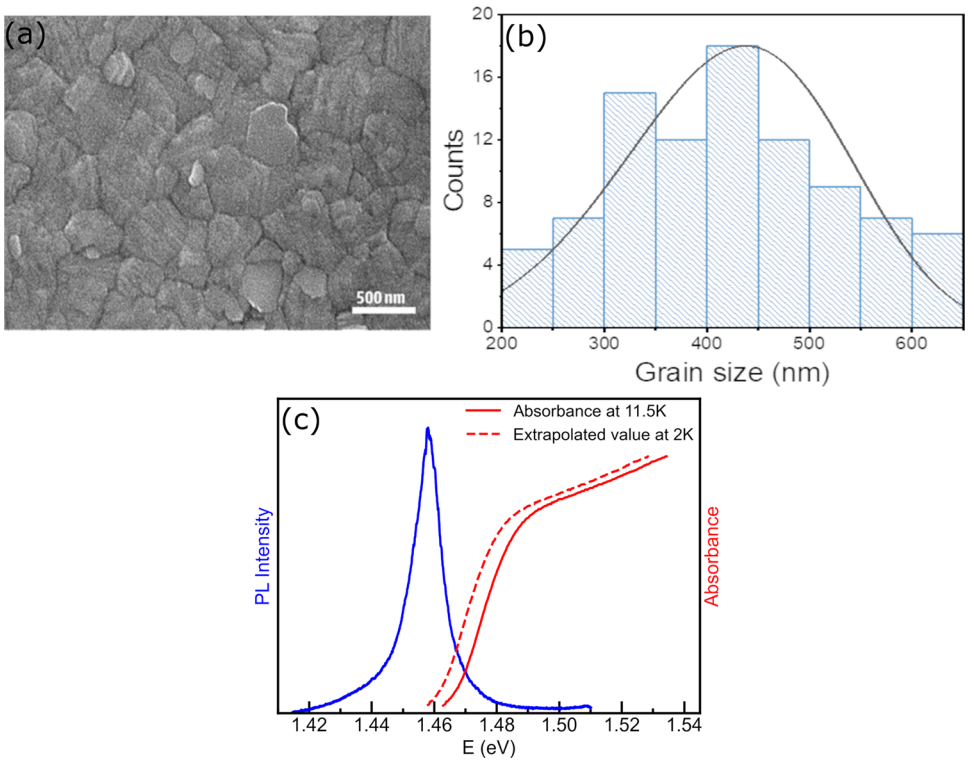

Figure 1. (a) SEM image of a $FAPbI_3$ film. (b) Grain size distribution in the film. (c) Photoluminescence and absorption spectra of a $FAPbI_3$ film.

optoelectronic domain but also in the less explored spintronic field due to its large spin−orbit coupling and its spin-dependent optical selection rules.

This work is the result of the collaboration of a team of chemists and two teams of experimental and theoretical physicists. We were able to obtain highly stable polycrystalline thin films of $FAPI_3$ prepared under air ambient conditions. In these materials, the presence of Pb−O bonds retains the propagation of α- to δ-$FAPbI_3$ phase conversion[18] and allowed addressing the study of the spin coherence and spin relaxation dynamics of the photoexcitations. We used time-resolved pump−probe Faraday rotation spectroscopy at low temperature (2 K) and, by applying a magnetic field perpendicular (parallel) to the film plane, we measured long living spin relaxation (spin decoherence) signals, extracting spin lifetimes similar to other HP single crystals, Landé factors, and their inhomogeneous broadenings. Under these experimental conditions, the average lifetime of samples was larger than seven months. We clearly identified two contributions to the Larmor spin precession that we associated with localized electrons and holes. From the measured hole g-factors and low-temperature absorption spectrum of $FAPbI_3$, we were able to obtain the Kane energy parameter of $FAPbI_3$, E_P = 13.1 eV. This is a key parameter to define the interaction of HP with magnetic fields and also describe the band structure and optical properties in the framework of the **k.p** theory and effective mass approximation,[19] applicable not only for bulk materials but also for nanostructures. This experimentally estimated value in $FAPbI_3$ is very close to the theoretical value calculated in this work and in our previous work,[20] although slightly smaller. Furthermore, it is in the range of the recently calculated and experimentally determined values in other Pb-based HP, between 11 and 20 eV.[11,19,20]

RESULTS AND DISCUSSION

The $FAPbI_3$ films were prepared according to a previously reported method,[18] where the $FAPbI_3$ perovskite solar cells presented an outstanding stability in air, retaining 80% of their initial power conversion efficiency after 112 days of storage in air. In this case, the films were fabricated under ambient air conditions, which creates a Pb−O bond and, through a deep study of Raman, XPS, and morphological analyses, indicates that the presence of Pb−O bonds blocks the expansion of the δ-FAPI phase, stabilizing the FAPI black phase. These findings suggested that the fabrication under ambient conditions intrinsically forms Pb−O bonds, likely PbOx species, which would improve the air stability. Figure 1a shows a top view obtained by scanning electron microscopy (SEM) of a 300 nm thick polycrystalline $FAPbI_3$ film. The grain size distribution is given in Figure 1b. The mean grain size is located around 400−450 nm. The film fabrication is described in more details in the Supporting Information S1.

The α-phase of $FAPbI_3$ is a perovskite cubic phase showing a direct gap located at the R point of the Brillouin zone at room temperature. $FAPbI_3$ undergoes a structural phase transition around 100−150 K when cooled down. A signature of this phase transition is clearly observed in the low-temperature absorption spectra (see Supporting Information S2 Figure S1). Below 150 K, the crystal adopts the tetragonal space group P4/mbm,[21] with the D_{4h} point group. Figure 1c shows the absorption spectrum obtained at 11.5 K and its extrapolation at 2 K, as well as the photoluminescence (PL) spectrum of a $FAPbI_3$ polycrystalline film obtained at 2 K and excited at 1.512 eV. From the absorption spectrum, the exciton energy can be experimentally determined (1.482 eV at 11.5 K). In a previous work, the binding energy for this material was determined to be equal to 14 meV[22] at low temperature. We can then deduce the energy gap is 1.496 eV. The PL maximum

https://doi.org/10.1021/acsphotonics.4c00632
ACS Photonics XXXX, XXX, XXX−XXX

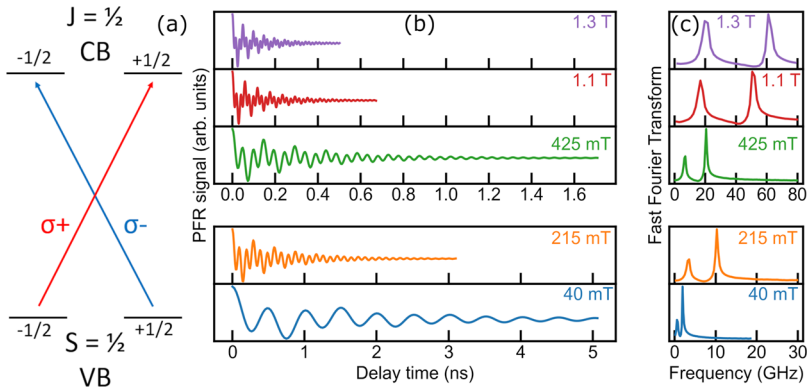

Figure 2. (a) Schematic of the optical selection rules when the laser energy is tuned to the band gap energy of bulk $FAPbI_3$, (b) PFR signal measured at different magnetic fields in Voigt geometry, and (c) fast Fourier transform of the PFR signals, revealing two frequencies.

is slightly shifted to lower energies (1.459 eV). The time-resolved PL detected at 1.5 eV and 4 K is weak and shows two decay times, 70 and 262 ps, and as we will discuss later, a more intense PL at lower energies arises very likely from localized states and defects (see Supporting Information S2 for more details on experimental methods and complementary experiments).

An efficient spin polarization in HP is obtained via optical orientation. Indeed, the conduction band minimum is a spin−orbit split-off band associated with Pb p-orbitals and characterized by a total angular momentum $j = 1/2$. At higher energy, we find the light and heavy electron bands with a total angular momentum $j = 3/2$. The valence band maximum with s symmetry and $S = 1/2$ is the result of a combination of Pb s-orbitals and I p-orbitals. The absorption of circularly polarized photons tuned to the band gap energy allows the selective pumping of spin-polarized electrons and holes in the HP material, based on optical selection rules and conservation of spin angular momentum. Figure 2a presents a schematic view of the optical selection rules for circularly polarized lights tuned to the band gap energy in HP. To study the spin decoherence and relaxation dynamics, we use a degenerated pump−probe experimental setup that allows the measurement of the photoinduced Faraday rotation (PFR) (see Supporting Information, S3, for more experimental details). The circularly polarized pump is tuned to 1.48 eV, and thanks to the optical selection rules, we can create circularly polarized excitons. The presence of spin-polarized carriers or excitons in the sample induces a rotation of the polarization plane of the linearly polarized probe beam. We measure this rotation, the PFR signal, as a function of the pump−probe delay. Figure 2b shows the PFR signals obtained at 2 K in an external magnetic field applied in Voigt configuration (perpendicular to the laser beams), when the energy is tuned to the maximum of the absorption edge at 1.48 eV. The Fourier transform (FFT) of the PFR signal for different values of the applied magnetic field is given in Figure 2c. Two frequencies are clearly identified, and both increase linearly as the magnetic field increases, which seems to be a very common feature in HP[6,11] (S3 in Supporting Information contains PFR results when the laser beams are tuned to 1.47 eV). The PFR signal can be described as two damped oscillations:

$$\theta_F = A_e e^{-t/T^*_{2,e}} \cos(2\pi f_e t + \varphi_e) + A_h e^{-t/T^*_{2,h}} \cos(2\pi f_h t + \varphi_h) \quad (1)$$

where f_i (i = e, h) are the two oscillation frequencies identified in the FFT; the low-frequency amplitude is noted as A_h and the high-frequency one as A_e, $T^*_{2,i}$ (i = e, h) is the dephasing time at a given magnetic field, and φ_i is the initial phase. These two components correspond to the localized carriers, electrons (i = e) and holes (i = h), and the two frequencies are their respective Larmor frequencies. We will discuss later why we assign the high frequency to electrons and the low frequency to holes. The pump beam creates excitons in $FAPbI_3$, but these excitons relax via a very fast path to localized centers and defects. That is why the cw-PL is shifted toward lower energies with respect to the absorption edge; the PL detected at 1.5 eV, as we have already written, is weak and shows two decay times, one equal to 262 ps and one, faster, of 70 ps. This latter faster decay is very likely associated with the relaxation time of free exciton to more localized states (see Supporting Information S2, Figure S3).

Figure 3a shows the PFR signal obtained at 2 K and 1.48 eV for an applied magnetic field of 1.1 T, fitted by eq 1, with the two carrier contributions extracted from the numerical fit. Figure 3b represents the dephasing time for electrons and holes as a function of magnetic field. They shorten with increasing magnetic field due to the g-factor inhomogeneities. Similar results are obtained when pump and probe energy are tuned to lower energy (see Supporting Information S3 Figure S4). The g-factor distribution width, Δg_i, and the spin dephasing time extrapolated at zero magnetic field for a single electron or hole can be determined using the relation:

$$\frac{1}{T^*_{2,i}} = \frac{1}{T_{2,i}(0)} + \frac{\Delta g_i \mu_B B}{\hbar} \quad (2)$$

where $T_{2,i}(0)$ is also equal to the longitudinal electron or hole spin relaxation time at zero magnetic field, μ_B is the Bohr magneton, and $\hbar$ is the reduced Planck constant. We extrapolate, at zero magnetic field and T = 2 K, a value $T_{2,e}(0) = 3.3 \pm 0.6$ ns for electrons and $T_{2,h}(0) = 2.4 \pm 0.8$ ns for holes. These values compare well with values found in the crystal alloy $FA_{0.9}Cs_{0.1}PbBr_{0.2}I_{2.8}$[23] and other HP crystals (see Supporting Information S4, Tables S1 and S2 contain a review of the experimental results known to date) but are much larger than the value obtained in $MA_{0.3}FA_{0.7}PbI_3$ thin films.[25] We found $\Delta g_e = 0.058$ ($\Delta g_h = 0.087$), representing 1.7% (7.7%) of the experimentally determined value of g_e(g_h). The relative dispersion is larger for the hole than for the electron, but both dispersions are smaller than the dispersions obtained in other

https://doi.org/10.1021/acsphotonics.4c00632
ACS Photonics XXXX, XXX, XXX−XXX

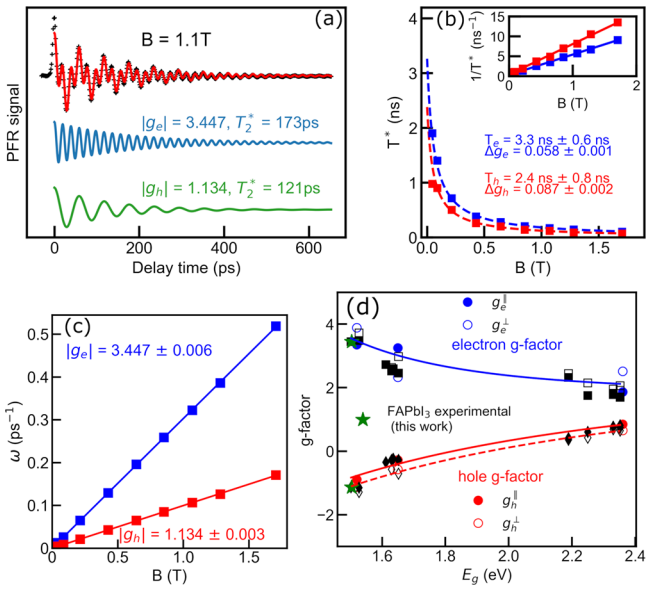

Figure 3. (a) PFR signal of $FAPbI_3$ thin film at B = 1.1 T, fit to expression 1. The electron and hole components are represented separately. (b) Evolution of spin dephasing times of charge carriers with the magnetic field. (c) Electron and hole Larmor frequencies as a function of magnetic field. (d) Red (blue) circles: theoretical hole (electron) g-factors for $FAPbI_3$, $MAPbI_3$, and $CsPbBr_3$. Black symbols: experimentally measured g-factors (see in S4 Tables S1 and S2). Empty (full) black symbols are for the minimum (maximum) g-values. Theoretical lines: blue line is a guide for the eyes corresponding to $\frac{g_e^{\parallel}+g_e^{\perp}}{2}$. Red lines represent $g_h^{\parallel}$ and $g_h^{\perp}$

HP films[5,6,25] and comparable with values obtained by other authors in crystals.[7,8,23]

Figure 3c shows the Larmor frequency:

$$\omega_i = 2\pi f_i = \frac{|g_i|\mu_B B}{\hbar} \tag{3}$$

where $|g_i|$ is the absolute value of the Landé factor of electron or hole, and B is the applied magnetic field. The results given in Figure 3c follow a linear behavior that shows no offset at zero magnetic field, confirming the involvement of a resident carrier rather than an exciton.[5] In the presence of an exciton, a finite frequency at B = 0 would be expected due to the electron−hole exchange interaction for carriers bound to an exciton. $|g_i|$ is deduced from the linear fits. They are comparable with the values obtained by other authors in $MA_{0.3}FA_{0.7}PbI_3$[24] and $FA_{0.9}Cs_{0.1}PbI_{2.8}Br_{0.2}$.[11] As $FAPbI_3$ has the lowest energy band gap in the Pb-based HP family, the quasi-cubic[11] and tetragonal **k.p** models[19] predict that the electron Landé factor in this material should have the highest value among the Pb-based HP. The hole Landé factor is predicted to be negative for $FAPbI_3$ and also has the highest absolute value among Pb-based HP. Figure 3d shows the hole and electron Landé factor values for Pb-based HP calculated with 14-band tetragonal model. (see Supporting Information S5, for more details about the calculations of the Landé factors values). For holes, in Figure 3d, we provide two lines representing a universal law of $g_h^{\parallel}$ and $g_h^{\perp}$ as a function of the gap energy E_g, and where $E_2 = 0.45E_g + 2.64$ and $E_3 = 0.45E_g + 2.79$ in eq 5 given in S5, and the two Kane parameters are considered $E_{P_{S,\rho}} \approx E_{P_{S,z}} = E_P = 12.4$ eV in the whole domain from 1.5 to 2.5 eV. Unlike the hole Landé factors, the electron Landé factors are sensitive to the coupling to other bands than the ones we considered, and for this reason, we provide a guide for the eyes, considering the arithmetic mean $\frac{g_e^{\parallel}+g_e^{\perp}}{2}$. Experimental values are also represented and show a very good agreement with theoretical calculations (see Supporting Information S4, Tables S1, S2, and S4). In the case of polycrystalline films, the experimental values should be compared to an average value of the two Landé factor components, along ($g_i^{\parallel}$) and perpendicular ($g_i^{\perp}$) to the c-axis of the tetragonal structure, $g_i = (2\, g_i^{\perp} + g_i^{\parallel})/3$. For holes, this expression depends essentially on $E_{P_{S,\rho}}$, $E_{P_{S,z}}$, the band gap energy E_g, and the transition energies from the maximum of the valence band s = 1/2 to the two nondegenerate j = 3/2 bands, E_2 and E_3 (see in Supporting Information S5, Figure S5). The energy values E_g = 1.49 eV, E_2 = 3.23 eV, and E_3 = 3.35 eV of $FAPbI_3$ have been experimentally obtained by low-temperature absorption spectra (see Supporting Information Figure S2) and, when they are combined with our measured hole Landé factor, it becomes possible to deduce an average Kane energy parameter for $FAPbI_3$ of $E_{P_{S,\rho}} \approx E_{P_{S,z}} = E_P$ = 13.1 eV (see S5 I). This value is slightly smaller than the one calculated in the framework of **k.p** theory and the tetragonal model for $FAPbI_3$ in this work (see S5 Table S3, $\tilde{E}_P = \frac{2E_{P_{S,\rho}} + E_{P_{S,z}}}{3} \approx 14.7$ eV), and smaller than the value calculated in our previous work[20] ($E_{P_{S,\rho}}$ = 17.97 eV and $E_{P_{S,z}}$ = 16.45 eV), but slightly larger than the average value of E_P = 12.4 eV obtained for HP with band gap energy between 1.5 and 2.5 eV. This latter value was deduced, as explained above, from the fit of the hole g-factor expressions given by the tetragonal model described in S5 (taking the phase angle θ = 40°) and the experimental results for hole g-factors, (see red lines in Figure 3d).

Finally, we have also measured the PFR signal in the presence of an applied magnetic field in Faraday configuration (magnetic field parallel to the beam propagation direction). Figure 4a shows the PFR signal obtained at 2 K and 1.48 eV for different longitudinal magnetic fields. These curves follow a multiexponential decay, as we can see in Figure 4b. The PFR signal at negative time values corresponds to the signal at the end of the previous pump/probe pulse, as shown in the schematic in Figure 4a. The delay between two pulses being 13.2 ns, the values at negative times were shifted by 13.2 ns to obtain the fits in Figure 4b. At B = 0, the PFR curve is well-described by two exponentials with characteristic times around a hundred of picoseconds and one or two nanoseconds. The shorter time is associated with free or localized excitons, and the slower one to the spin relaxation time, τ_1, of localized electrons and holes. We underline that the latter value is comparable to the value obtained for $T_{2,e/h}(0)$. τ_1 evolves as a function of the strength of the applied magnetic field, as shown in Figure 4c. We estimated its value to 17 ns for a magnetic field of 32 mT, a value comparable to the relaxation times obtained in other HP crystals[7,10,16] (see Supporting Information S4, Table S1). We observe that a very small value of the magnetic field is able to induce an increase of the relaxation time τ_1 by an order of magnitude, which is a signature of a quenching of relaxation channels, most likely due to the hyperfine interaction.[16] The maximum value of τ_1 is relatively constant from 20 to 200 mT.

https://doi.org/10.1021/acsphotonics.4c00632
ACS Photonics XXXX, XXX, XXX−XXX

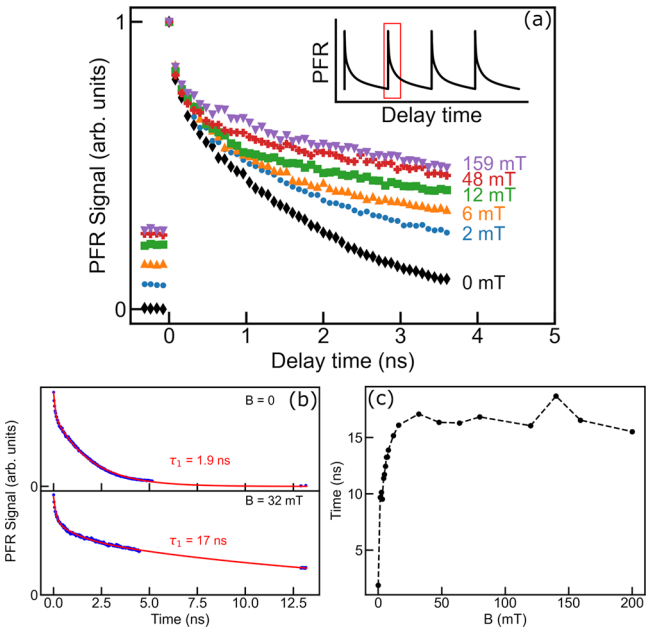

Figure 4. PFR signal in the presence of an applied magnetic field in Faraday geometry. (a) PFR signal at different magnetic fields. Inset: periodic PFR signal with period equal to 13,2 ns. The red square provides the window of the measured signal. (b) PFR signal at $B = 0$ and $B = 32$ mT, fitted with three exponential decays. (c) Field dependence of the longest decaying time τ_1

CONCLUSIONS

In summary, we studied the spin dynamics of resident electrons and holes in $FAPbI_3$ films that show high stability with time (no signatures of PFR signal degradation were observed for times longer than 7 months). The spin dephasing times, 3.3 ns for electrons and 2.4 ns for holes, are comparable with dephasing times measured in other Pb-based HP crystals and, in general, larger than the time measured in polycrystalline films. The longitudinal spin relaxation time of carriers increases from 2 ns at zero magnetic field to more or less 17 ns at 32 mT and stays constant until approximately 200 mT. The observed increase at very low longitudinal magnetic fields is very likely, as demonstrated in other Pb-based HP materials, due to the quenching of the hyperfine interaction. As predicted by cubic and tetragonal **k.p** models, the absolute values of Landé factors in $FAPbI_3$ are among the highest in the Pb-based HP family. We showed, in particular, that a 14-band tetragonal **k.p** model could describe the anisotropy of the hole g factors in the whole range of the Pb-based HP, which is in agreement with the ensemble of the experimental results known to date. By completing the range of studied materials, this work contributes to draw a general picture of spin dynamics in Pb-based HP.

From the measured hole Landé factors and experimental ellipsometry results found in the literature, we obtained an average Kane energy value $E_P = 13.1$ eV, slightly smaller than the one calculated. This is a key parameter to determine the optical properties of $FAPbI_3$ material and its magnetic interactions. All these results, making a connection between spin properties and optoelectronic properties, are of prime importance to evaluate the potentialities of $FAPbI_3$ as a future actor in engineered HP spin-optronic devices.

ASSOCIATED CONTENT

Supporting Information

The Supporting Information is available free of charge at https://pubs.acs.org/doi/10.1021/acsphotonics.4c00632.

S1: sample preparation; S2: absorption and photoluminescence measurements; S3: photoinduced Faraday rotation measurements; S4: experimental results in halide perovskite: Landé factors, dephasing, and relaxation times; and S5: tetragonal **k.p** model in D_{4h} point group (PDF)

AUTHOR INFORMATION

Corresponding Author

Maria Chamarro − *Sorbonne Université, CNRS, Institut des Nanosciences, Paris 75005, France*; Email: maria.chamarro@insp.jussieu.fr

Authors

Guillaume Lagüe − *Sorbonne Université, CNRS, Institut des Nanosciences, Paris 75005, France*

Frederick Bernardot − *Sorbonne Université, CNRS, Institut des Nanosciences, Paris 75005, France*

Victor Guilloux − *Sorbonne Université, CNRS, Institut des Nanosciences, Paris 75005, France*

Laurent Legrand − *Sorbonne Université, CNRS, Institut des Nanosciences, Paris 75005, France*; orcid.org/0000-0002-9465-1482

Thierry Barisien − *Sorbonne Université, CNRS, Institut des Nanosciences, Paris 75005, France*; orcid.org/0000-0003-1814-5948

Jesús Sánchez-Diaz − *Institute of Advanced Materials (INAM), Universitat Jaume I, Castelló de la Plana 12071, Spain*

Sergio Galve-Lahoz − *Institute of Advanced Materials (INAM), Universitat Jaume I, Castelló de la Plana 12071, Spain*

Imen Saïdi − *Université de Carthage, Faculté des Sciences de Bizerte, LR01ES15 Laboratoire de Physique des Matériaux: Structure et Properties, 7021 Bizerte, Tunisia*

Kais Boujdaria − *Université de Carthage, Faculté des Sciences de Bizerte, LR01ES15 Laboratoire de Physique des Matériaux: Structure et Properties, 7021 Bizerte, Tunisia*

Juan P. Martinez-Pastor − *UMDO, Instituto de Ciencia de los Materiales, Universidad de Valencia, Paterna 46980 Valencia, Spain*

Christophe Testelin − *Sorbonne Université, CNRS, Institut des Nanosciences, Paris 75005, France*

Iván Mora-Seró − *Institute of Advanced Materials (INAM), Universitat Jaume I, Castelló de la Plana 12071, Spain*; orcid.org/0000-0003-2508-0994

Complete contact information is available at: https://pubs.acs.org/10.1021/acsphotonics.4c00632

Notes

The authors declare no competing financial interest.

ACKNOWLEDGMENTS

This work was supported by the French National Research Agency (ANR IPER-Nano2, ANR-18-CE30-0023) and the French Ministry of Foreign Affairs for funding through the project PHC-Utique (CMCU 22G1305). F.B., M.C., and G.L.

thank Samuel Der for discussions on the applications of the **k.p** tetragonal model used in this work.

REFERENCES

(1) NREL. *Best Research-Cell Efficiencies Chart*. URL https://www.nrel.gov/pv/cell-efficiency.html (accessed 2024-06-27).
(2) Quan, L. Q.; Rand, B. P.; Friend, R. H.; Mhaisalkar, S. G.; Lee, T. W.; Sargent, E. H. Perovskites for next generation optical sources. *Chem. Rev.* **2019**, *119* (12), 7444−7477.
(3) Zhu, H.; Fu, Y.; Meng, F.; Wu, X.; Gong, Z.; Ding, Q.; Gustafsson, M. V.; Trinh, M. T.; Jin, S.; Zhu, X.-Y. Lead halide perovskite nanowire lasers with low lasing thresholds and high quality factors. *Nat. Mater.* **2015**, *14*, 636−642.
(4) Givonni, D.; Ma, H.; Chua, J.; Grätzel, M.; Ramesh, R.; Mhaisalkar, S.; Mathews, N.; Sum, T. C. Highly spin-polarized carriers dynamics and ultralarge magnetization in $CH_3NH_3PbI_3$ perovskite thin films. *Nano Lett.* **2015**, *15* (3), 1555−1558.
(5) Odenthal, P.; Talmadge, W.; Gundlach, N.; Wang, R.; Zhang, C.; Sun, D.; Yu, Z.-G.; Valy Vardeny, Z.; Li, Y. S. Spin-polarized exciton quantum beating in hybrid organic−inorganic perovskites. *Nat. Phys.* **2017**, *13*, 894−899.
(6) Garcia-Arellano, G.; Trippe-Allard, G.; Legrand, L.; Barisien, T.; Garrot, D.; Deleporte, E.; Bernardot, F.; Testelin, C.; Chamarro, M. Energy tuning of electronic spin coherent evolution in methylammonium lead iodide perovskites. *J. Phys. Chem. Lett.* **2021**, *12*, 8272−8279.
(7) Kirstein, E.; Yakovlev, D. R.; Zhukov, E. A.; Höcker, J.; Dyakonov, V.; Bayer, M. Spin dynamics of electrons and holes interacting with nuclei in $MAPbI_3$ perovskite single crystals. *ACS Photonics* **2022**, *9*, 1375−1384.
(8) Huynh, U. N.; Liu, Y.; Chanana, A.; Khanal, D. R.; Sercel, P. C.; Huang, J.; Vardeny, Z. V. Transient quantum beatings of trions in hybrid organic tri-iodine perovskite single crystal. *Nat. Commun.* **2022**, *13*, 1428.
(9) Garcia-Arellano, G.; Trippe-Allard, G.; Campos, T.; Bernardot, F.; Legrand, L.; Garrot, D.; Deleporte, E.; Testelin, C.; Chamarro, M. Unexpected anisotropy of the electron and hole Lande g-factors in perovskite $CH_3NH_3PbI_3$ polycrystalline films. *Nanomaterials* **2022**, *12*, 1399.
(10) Belykh, V. V.; Yakovlev, D. R.; Glazov, M. M.; Grigoryev, P. S.; Hussain, M.; Rautert, J.; Dirin, D. N.; Kovalenko, M. V.; Bayer, M. Coherent spin dynamics of electrons and holes in CsPbBr3 perovskite crystals. *Nat. Commun.* **2019**, *10*, 673.
(11) Kirstein, E.; Yakovlev, D. R.; Glazov, M. M.; Zhukov, E. A.; Kudlacik, D.; Kalitukha, I. V.; Sapega, V. F.; Dimitriev, G. S.; Semina, M. A.; Nestoklon, M. O.; Ivchenko, E. L.; Kopteva, N. E.; Dirin, D. N.; Nazarenko, O.; Kovalenko, M. V.; Baumann, A.; Höcker, J.; Dyakonov, V.; Bayer, M. The Lande factors of electrons and holes in lead halide perovskites: universal dependence on the band gap. *Nat. Commun.* **2022**, *13*, 3062.
(12) Kirstein, E.; Kopteva, N. E.; Yakovlev, D. R.; Zhukov, E. A.; Kolobkova, E. V.; Kuznetsova, M. S.; Belykh, V. V.; Yugova, I. A.; Glazov, M. M.; Bayer, M.; Greilich, A. Mode locking of hole spin coherences in $CsPb(Cl, Br)_3$ perovskite nanocrystals. *Nat. Comm.* **2023**, *14*, 699.
(13) Kirstein, E.; Smirnov, D. S.; Zhukov, E. A.; Yakovlev, D. R.; Kopteva, N. E.; Dirin, D. N.; Hordiichuk, O.; Kovalenko, M. V.; Bayer, M. The squeezed dark nuclear spin state in lead halide perovskites. *Nat. Commun.* **2023**, *14*, 6683.
(14) Xuyang, L.; Yaoyao, H.; Jingyi, Z.; Kaifeng, W. Room-temperature coherent optical manipulation of hole spins in solution-grown perovskite quantum dots. *Nat. Nanotechnol.* **2023**, *18*, 124−130.
(15) Shumitskaya, A. A.; Kozlov, V. O.; Selivanov, N. I.; Stoumpos, C. C.; Zapasskii, V. S.; Kapitonov, Y. V.; Ryzhov, I. I. The Faraday effect and phase transition in the $CH_3NH_3PbI_3$ halide perovskite single crystal. *Adv. Opt. Mater.* **2023**, *12*, No. 2302095.
(16) Kirstein, E.; Yakovlev, D. R.; Glazov, M. M.; Evers, E.; Zhukov, E. A.; Belykh, V. V.; Kopteva, N. E.; Kudlacik, D.; Nazarenko, O.; Dirin, D. N.; Kovalenko, M. V.; Bayer, M. Lead-dominated hyperfine interaction impacting the carrier spin dynamics in halide perovskites. *Adv. Mater.* **2022**, *34*, No. 2105263.
(17) Masi, S.; Gualdrón-Reyes, A. F.; Mora-Seró, I. Stabilization of Black Perovskite Phase in $FAPbI_3$ and $CsPbI_3$. *ACS Energy Lett.* **2020**, *5* (6), 1974−1985.
(18) Salim, K. M. M.; Masi, S.; Gualdon-Reyes, A. F.; Sanchez, R. S.; Barea, E. M.; Krêsmarovà, M.; Sanchez-Roy, J. F.; Mora-Serò, I. Boosting long-term Stability of pure Formamidinium perovskte solar cells by ambient air additive assisted fabrication. *ACS Energy Lett.* **2021**, *6* (10), 3511−3521.
(19) Garcia-Arellano, G.; Boujdaria, K.; Chamarro, M.; Testelin, C. Lande g-factors in tetragonal halide perovskite: a multiband k.p model. *Phys.Rev. B* **2022**, *106* (16), No. 165201.
(20) Ben Aich, R.; Ben Radhia, S.; Boujdaria, K.; Chamarro, M.; Testelin, C. Multiband k·p Model for Tetragonal Crystals: Application to Hybrid Halide Perovskite Nanocrystals. *J. Phys. Chem. Lett.* **2020**, *11*, 808−817.
(21) Weber, O. J.; Ghosh, D.; Gaines, S.; Henry, P. F.; Walker, A. B.; Islam, M. S.; Weller, M. T. Phase behaviour and Polymorphism of Formamidinium Lead Iodide. *Chem. Mater.* **2018**, *30* (11), 3768−3778.
(22) Baranowski, M.; Plochocka, P.; Su, R.; Legrand, L.; Barisien, T.; Bernardot, F.; Xiong, Q.; Testelin, C.; Chamarro, M. Exciton Binding Energy and Effective Mass of $CsPbCl_3$: a Magneto-Optical Study. *Photon. Res.* **2020**, *8*, A50−A55.
(23) Kirstein, E. *Coherent spin dynamics and carrier-nuclear interaction in lead halide perovskite crystals*; TU Dortmund: Dortmund, Germany, 2022.
(24) Zhang, H.; Zhai, Z.; Bi, Z.; Gao, H.; Ye, M.; Xu, Y.; Tan, H.; Yang, L. Spin Coherence and spin relaxation in hybrid organic-inorganic lead and mixd lead-tin perovskites. *Nano Lett.* **2023**, *23*, 7914−7920.
(25) Jacoby, L. M.; Crane, M. J.; Gamelin, D. R. Coherent spin dynamics in vapor-deposited CsPbBr3 perovskite thin films. *Chem. Mater.* **2022**, *34*, 1937−1945.

https://doi.org/10.1021/acsphotonics.4c00632
ACS Photonics XXXX, XXX, XXX−XXX